metals

MDPI

Communication

Effect of Water Jet Cavitation Peening on Short-Period Oxidation Behavior of Alloy 600 in PWR Primary Water

Tingyun Ming [1,2], Qunjia Peng [2,*], Yaolei Han [2] and Tao Zhang [3,*]

[1] College of Materials Science and Chemical Engineering, Harbin Engineering University, Harbin 150001, China
[2] Suzhou Nuclear Power Research Institute, Suzhou 215004, China
[3] Shenyang National Laboratory for Materials Science, Northeastern University, Shenyang 110819, China
* Correspondence: qunjiapeng@163.com (Q.P.); zhangtao@mail.neu.edu.cn (T.Z.)

Abstract: Water jet cavitation peening (WJCP) was used to strengthen the surface of nickel-based alloy 600. Residual stress, hardness, surface roughness, microstructure, and short-period oxidation behavior in untreated (UT) and WJCP-treated alloy 600 were characterized. A continuous oxide film was formed on the WJCP-treated surface after a short period of exposure, while it was discontinuous in the UT specimen. The change in oxidation behavior was attributed to the ultrafine grain and dislocation structure resulting from the WJCP treatment.

Keywords: oxidation; high-temperature water; water jet cavitation peening; microstructure

check for updates

Citation: Ming, T.; Peng, Q.; Han, Y.; Zhang, T. Effect of Water Jet Cavitation Peening on Short-Period Oxidation Behavior of Alloy 600 in PWR Primary Water. *Metals* **2023**, *13*, 336. https://doi.org/10.3390/met13020336

Academic Editor: Tomáš Prošek

Received: 9 December 2022
Revised: 15 January 2023
Accepted: 17 January 2023
Published: 8 February 2023

Copyright: © 2023 by the authors. Licensee MDPI, Basel, Switzerland. This article is an open access article distributed under the terms and conditions of the Creative Commons Attribution (CC BY) license (https://creativecommons.org/licenses/by/4.0/).

1. Introduction

Stress corrosion cracking (SCC) is one major failure mode for nickel-based alloy 600 components in pressurized water reactor (PWR) primary water [1–3]. The slip-dissolution/oxidation and internal oxidation models suggested that oxidation plays a significant role in the crack initiation stage [4]. Extensive investigations have been conducted to study the effect of oxidation on the SCC of steel in PWR primary water. It can be found that oxide scales had a double-layer structure [4–6] in which the inner Cr-rich oxide films could further affect the SCC behavior of the steels. A continuous and dense inner oxide film helped mitigate or slow the oxidation and SCC of the materials; however, a discontinuous and porous one may promote further oxidation and SCC.

To date, some researchers studied the effect of surface peening on the SCC of alloy 600 [7,8]. Similar conclusions of superior SCC resistance in the peened alloy were found, which was extensively attributed to the introduction of residual compressive stress. The influence of peening was seen in the microstructure upon oxidation and SCC; however, it was not well understood. Lu et al. [9] pronounced that refined grains could enhance the probability of crack arrest at the triple junction of grain boundaries. Another study [10] pointed out that the micro-current coupling strength between refined grain boundaries and grains was less than that in coarse-grain counterparts, which could improve the SCC resistance of 304 stainless steel. Nevertheless, refined grains possess a higher grain boundary density, which may promote the SCC of the alloy. According to [11], some micro-cracks may be formed in 316 L stainless steel after shot peening treatment; it may increase the SCC susceptibility of the steel. Lopez-Ruiz [12] found that shot peening could introduce martensite transformation and pellet residue, which may cause galvanic corrosion between austenitic and martensite and pellet residue contaminations. Similarly, some studies suggested that the corrosion resistance of 316 L stainless steel was reduced after laser peening due to an increase in surface roughness. For alloy 600, Karthik and Swaroop [13] proved that laser shock peening could enhance the corrosion resistance of the alloy in NaCl solution, which was attributed to the formation of residual compressive stress. Extensive investigations were conducted; however, the effect of surface peening on the oxidation behavior of alloy 600 in high-temperature water was limited. According to [14,15],

WJCP is an environmentally friendly and economical surface peening technique compared with traditional shot peening and laser peening. It mainly strengthens the material via cavitation collapse shock waves. In addition, it is well-known that the oxidation of the alloy in high-temperature water for a short period is important for crack initiation [16]. Further investigation of the effect of water jet cavitation peening (WJCP) on the short-period oxidation behavior of the alloy is required. It may help clarify the mechanism of the peening-induced improvement of SCC resistance. Consequently, the effect of WJCP-induced changes in microstructure on the short-period oxidation behavior of Inconel 600 in PWR primary water was studied.

2. Materials and Methods

Mill-annealed nickel-based alloy 600 (600 MA) was used in the present work. Table 1 lists the chemical composition of the alloy. The plate specimens with a dimension of 10 mm × 10 mm × 1.5 mm were used to characterize the change in residual stress, hardness, surface roughness, microstructure, and the short-period oxidation behavior in 600 MA. All specimens were first polished up with 2000# SiC sandpaper and then polished with non-crystallizing colloidal silica polishing suspension (0.02 μm) for 2 h to remove the surface residual strain. Subsequently, the WJCP treatment was applied to the surface. The WJCP system shown in an earlier study [14] was utilized for to strengthen the surface of the alloy. The optimized WJCP parameters of a working pressure of 30 MPa, a standoff distance of 30 mm, a scanning rate of 0.3 mm/s, and a scanning pitch of 1 mm were applied to enhance the alloy.

Table 1. Chemical composition of nickel-based alloy 600 (wt. %).

Element	Cr	Fe	C	S	Mn	Si	Cu	Ni
Composition	16.79	8.29	0.033	<0.010	0.46	0.11	<0.010	Bal.

After the WJCP treatment, the residual stress, hardness, surface roughness, and the microstructure of the surface layer were characterized. The residual stress was evaluated with a Proto LXRD stress tester according to GB/T 7704-2017. A VK-X100K topography instrument was used to measure the surface roughness before and after the WJCP treatment. A Q10A+ Vickers hardness tester (Qness, Austria) was applied to test the change in surface hardness before and after the WJCP treatment. During the measurement of hardness, a load of 1000 gf, a loading time of 10 s, and an unloading time of 5 s were applied. The microstructure of the surface layer was characterized using a FEI Helios transmission electron microscope (TEM, FEI, USA). The TEM samples were extracted using an FEI Helios G4 UX focused ion beam (FIB) instrument (FEI, USA) from the WJCP-treated surface in 600 MA.

The short-period exposure experiment was conducted in simulated PWR primary water in a refreshed loop equipped with a 15 L autoclave made of 316 stainless steel. The PWR primary water was prepared with ultra-pure water with 1000 mg/L of B as H_3BO_3 and 2 mg/L of Li as $LiOH{\cdot}H_2O$. The temperature was 320 °C, the pressure was 13 MPa, the flow rate was about 100 mL/min, and the immersion period was 50 h. The dissolved oxygen was kept at less than 5 ppb, which was continuously monitored using an Inpro 7000-VP METTLER TOLEDO sensor at the autoclave inlet water. Similarly, the conductivity of the influent water was continuously monitored during the test using an InPro 6050 sensor.

After the exposure experiment, the untreated (UT) and WJCP-treated 600 MA were removed from the autoclave for the observation of the change in corrosion behavior. Before the observation, all specimens were ultrasonically cleaned with ultra-pure water and ethanol, which is consistent with our previous work [14]. The surface morphology was observed using a ZIEES Sigma 300 scanning microscope (SEM, ZIEES, Germany) at an operating potential of 20 kV. Subsequently, FIB was used to prepare the TEM specimens at

(111) orientation, which was marked by the combination of the hardness mark and electron backscatter diffraction (EBSD) measurement before the exposure experiment. Then, the cross-section morphology and the element composition of the oxide scales were analyzed using a TEM equipped with an energy-dispersive X-ray spectrometer (EDS). The structure of the oxide scales was analyzed from the EDS and the high-resolution TEM (HRTEM) images and the corresponding fast Fourier transformation (FFT).

3. Results and Discussion

3.1. Characterization of 600 MA after the WJCP Treatment

3.1.1. Residual Stress, Hardness, and Surface Roughness

After the WJCP treatment, residual compressive stress was introduced in 600 MA (Table 2); it was changed from 55 ± 18 MPa to −535 ± 25 MPa. In addition, increases in hardness and surface roughness could also be detected. The surface hardness was increased from 162.8 ± 3.5 HV to 201.2 ± 5.8 HV, and the surface roughness was increased from 1.3 ± 0.2 μm to 2.1 ± 0.3 μm. These results indicated that the alloy was severely plastic deformed.

Table 2. WJCP-induced changes in residual stress, hardness, and surface roughness in 600 MA.

Specimen	Residual Stress (MPa)	Hardness (HV)	Surface Roughness (μm)
UT	55 ± 18	162.8 ± 3.5	1.3 ± 0.2
WJCP	−535 ± 25	201.2 ± 5.8	2.1 ± 0.3

3.1.2. Microstructure

The cross-section TEM observation of the WJCP-induced surface deformation layer is illustrated in Figure 1. Compared with the UT specimen (Figure 1a), an ultrafine grain layer was formed on the top surface in WJCP-treated 600 MA (Figure 1b). Its thickness was about 100 nm, and the average grain size was about 30 nm. The sub-surface deformation layer was mainly composed of a dislocation structure (Figure 1c).

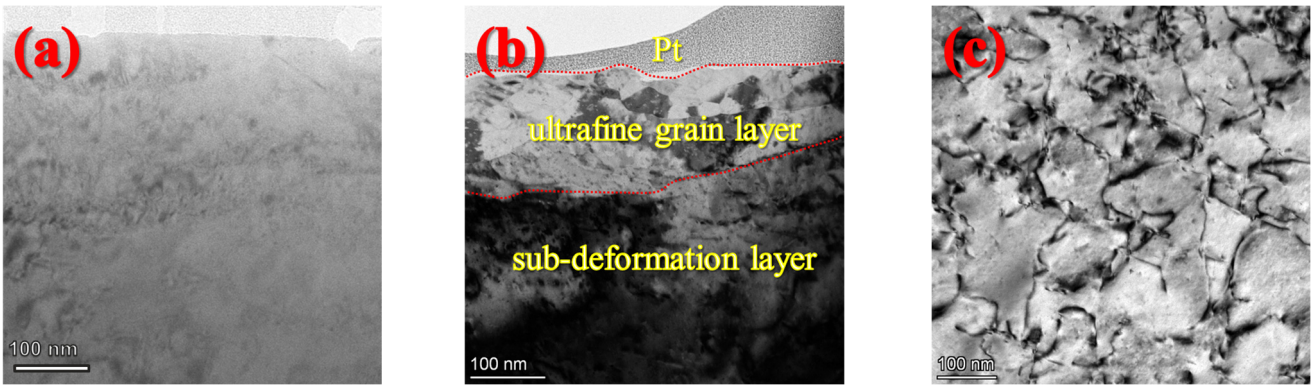


Figure 1. Cross-section TEM observation of the surface layer in UT (**a**) and WJCP-treated (**b**,**c**) 600 MA. (**b**) Surface ultrafine grain layer, (**c**) sub-surface dislocation structure.

3.2. Characterization of Oxide Scales after the Exposure Experiment

Figure 2 shows the surface morphology of oxide scales formed on the surface of UT and WJCP-treated 600 MA. The oxide scales were both granular-like and needle-like. The number of oxide particles and needle-like oxides in the WJCP-treated specimen was higher than that in the UT specimen.

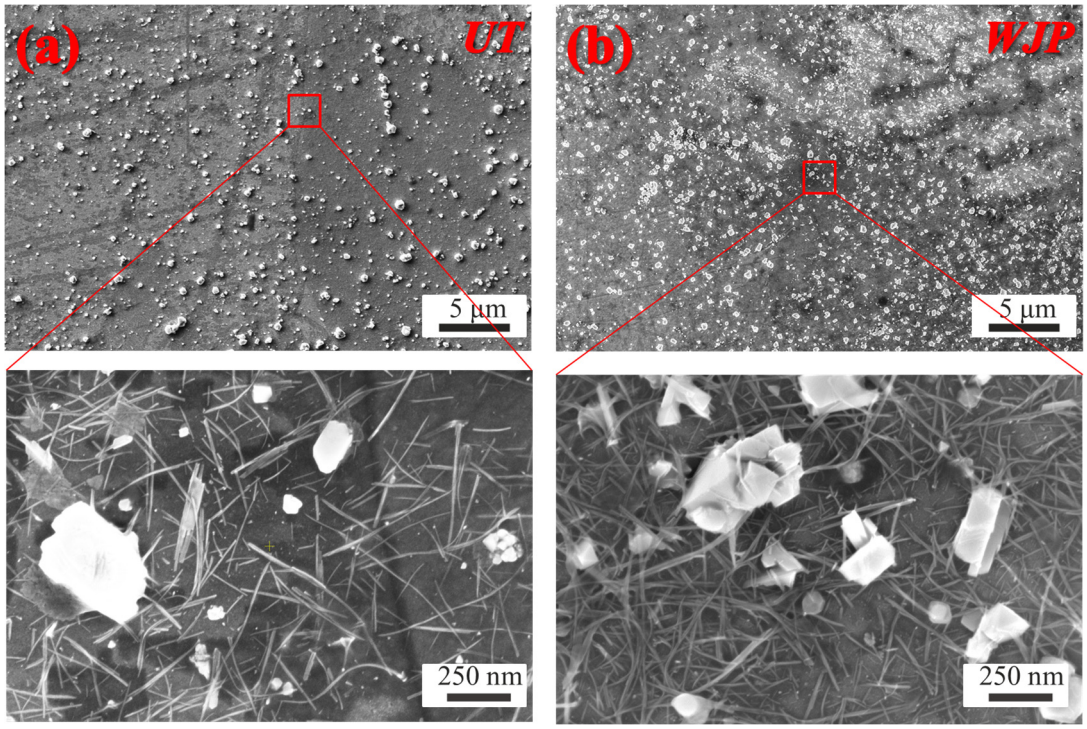


Figure 2. Surface morphology of 600 MA after the short-period exposure experiment. (**a**) UT, (**b**) WJP.

Figure 3 illustrates the cross-section morphology, element distribution, and structure of oxide scales formed in UT and WJCP-treated 600 MA. The STEM maps and corresponding EDS images suggested a typical double-layer structure of the oxide scales. A discontinuous oxide scale was formed in the UT specimen, while a continuous inner oxide film was formed on the WJCP-treated surface. This suggested that the WJCP-treated surface could be quickly oxidized and formed an intact oxide film. EDS maps confirmed that oxide scales with similar compositions were formed on the surface of UT and WJCP-treated 600 MA. The outer oxide particles were Cr-depleted, while the inner oxide films were Cr-rich. The thicknesses of the inner oxide films formed in UT and WJCP-treated 600 MA were similar; they were both about 30 nm.

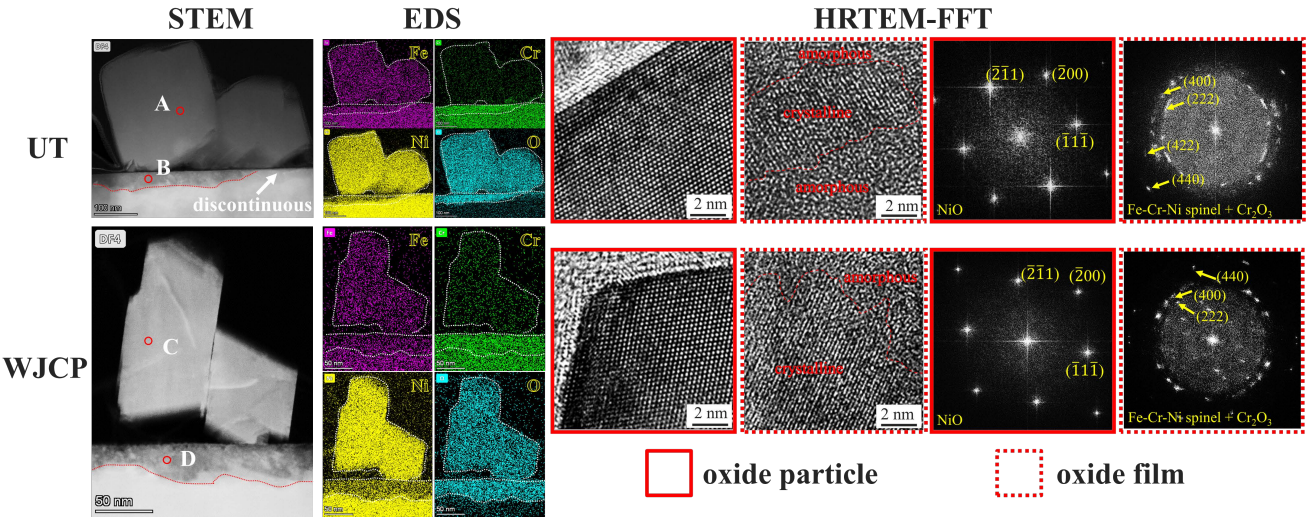


Figure 3. STEM-EDS and HRTEM-FFT of oxide scale formed on the surface of UT and WJCP-treated 600 MA.

To clarify the structure of the oxide scales formed in 600 MA, quantitative EDS and HRTEM-FFT were conducted. Combining the results of EDS (Table 3) and HRTEM-FFT (Figure 3), the outer oxide particles had a NiO structure, whereas the inner oxide films had an Fe-Cr-Ni spinel + Cr_2O_3 structure. This suggested that the WJCP treatment could only change the morphology of oxide scales; it did not change their chemical composition and phase structure. The thermodynamic–kinetics deposition sequence (Figure 4a) of oxide scales in 600 MA was calculated from the relationship among the Gibbs free energy, the change in entropy and heat capacity, and the solubility product of the oxide scales shown in an earlier investigation [14]. According to Figure 4a, the oxide scales formed on the surface of 600 MA should be the structure of Cr_2O_3 → Fe-Cr-Ni spinel → NiO (inner → outer). This well agrees with the EDS and HRTEM-FFT results.

Table 3. Chemical composition (at. %) and structure of the oxide scale formed on the UT and WJCP-treated surface.

Position	Fe	Cr	Ni	O	Structure
A	4.13	0.26	47.05	48.56	NiO
B	5.69	16.54	18.94	58.83	Fe-Cr-Ni spinel + Cr_2O_3
C	3.55	0.32	47.31	48.81	NiO
D	4.20	16.24	19.83	59.74	Fe-Cr-Ni spinel + Cr_2O_3

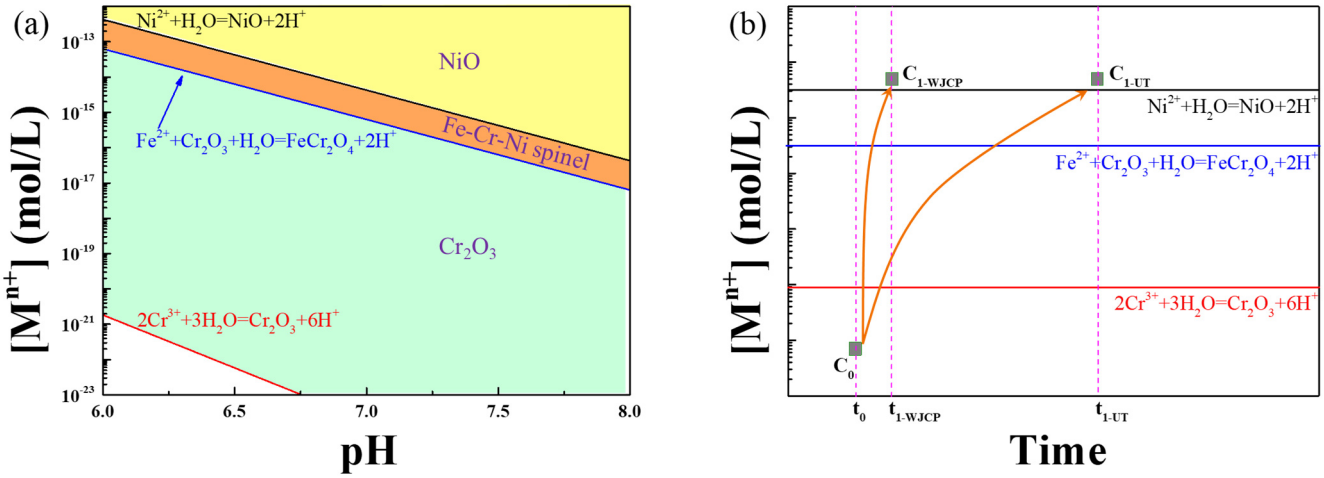


Figure 4. Thermodynamic–kinetics deposition sequence for the formation of oxide scales (**a**) and the schematic diagram of ion concentration change (**b**) in 600 MA.

The morphology difference of the inner oxide film in 600 MA was attributed to the WJCP-induced change in the microstructure of the surface layer. After the WJCP treatment, an ultrafine grain layer and many dislocations were formed. These microstructure changes could also promote the dissolution of the alloy [14]. Subsequently, the metal ion concentration quickly exceeded the critical value in a short time (Figure 4b), which was helpful for the nucleation of oxides. The nucleation rate (V_N) for the formation of oxide scales in unit time and unit area can be calculated from Equation (1) [17]:

$$V_N = ASexp(-\frac{16\pi v_0^2\gamma^3}{3k^3T^3ln^2S}) \quad (1)$$

in which A is a constant, 3.7×10^{-7} $cm^{-2}{\cdot}s^{-1}$; S is the supersaturation; v_0 is the molecular volume, 2×10^{-29} m^3; γ is the surface energy of critical nucleation size, 0.1 $J{\cdot}m^{-2}$; k is the Boltzmann constant, 13.8×10^{-23} $J{\cdot}K^{-1}$; T is the temperature, 595 K. After the WJCP treatment, S was increased and γ was decreased. Consequently, the nucleation rate was increased. In addition, the increase in surface roughness could also increase the real contact

area between surface and high temperature. It could enhance the dissolution and oxidation of the alloy [14,18]. As a result, a continuous oxide scale could be formed on the WJCP-treated surface. In addition, the increase in active sites of grain boundaries and dislocation could also promote the formation of oxides [18]. Thus, the density of oxide particles and needle-like oxides in WJCP-treated 600 MA was higher than that in the UT specimen (Figure 2). Chen et al. [19] studied the effect of rotationally accelerated shot peening on the corrosion resistance of 316LN stainless steel in 3.5 wt% NaCl solution. According to their investigation and our previous work [14], it was found that the peened specimens possessed a higher nucleation rate, which agrees with the present work.

4. Conclusions

600 MA was subjected to WJCP treatment, and residual compressive stress was introduced. An ultrafine grain layer and lots of dislocations were formed in the surface layer. A continuous inner oxide film was formed in WJCP-treated 600 MA after a short-period of exposure in the experiment, which was attributed to the WJCP-induced refined grain layer and dislocation structure. The refined grain layer and dislocation structures could change the dissolution of the alloy and further influence the oxidation behavior.

Author Contributions: T.M.—conceptualization, methodology, investigation, validation, writing—original draft, writing—review and editing. Q.P.—conceptualization, methodology, writing—review and editing, supervision, funding acquisition. Y.H.—validation. T.Z.—conceptualization, methodology, writing—review and editing. All authors have read and agreed to the published version of the manuscript.

Funding: This work was financially supported by the National Natural Science Foundation of China (No. 51901019) and the Liao Ning Revitalization Talents Program (No. XLYC2002071).

Data Availability Statement: Not applicable.

Conflicts of Interest: The authors declare no conflict of interest.

References

1. Lim, Y.S.; Hwang, S.S.; Kim, S.W.; Kim, H.P. Primary water stress corrosion cracking behavior of an alloy 600/182 weld. *Corros. Sci.* **2015**, *100*, 12–22. [CrossRef]
2. Min, S.; Liu, H.; Wang, J.; Hou, J. Early oxidation behavior of Ni-based Alloy 690 in simulated pressurized water reactor environment with varying surface conditions. *Corros. Commun.* **2021**, *4*, 68–81. [CrossRef]
3. Wu, X.; Liu, X.; Zhang, Z.; Tan, J.; Han, E.; Ke, W. Some fundamental understandings of Zn-injection water chemistry on material corrosion in pressurized water reactor primary circuit. *Corros. Commun.* **2022**, *6*, 52–61. [CrossRef]
4. Persaud, S.Y.; Langelier, B.; Korinek, A.; Ramamurthy, S.; Botton, G.A.; Newman, R.C. Characterization of initial intergranular oxidation processes in alloy 600 at a sub-nanometer scale. *Corros. Sci.* **2018**, *133*, 36–47. [CrossRef]
5. Wang, Z.H.; Takeda, Y. Mechanistic understanding of the roles of hydrogen in modification of oxide film of alloy 600 in high temperature high pressure water environment. *Corros. Sci.* **2020**, *170*, 108656. [CrossRef]
6. Wang, Z.H.; Takeda, Y. Amorphization and structural modification of the oxide film of Ni-based alloy by in-situ H charging in high temperature high pressure water environment. *Corros. Sci.* **2020**, *166*, 108474. [CrossRef]
7. Telang, A.; Gill, A.S.; Teysseyre, S.; Mannava, S.R.; Qian, D.; Vasudevan, V.K. Effects of laser shock peening on SCC behavior of alloy 600 in tetrathionate solution. *Corros. Sci.* **2015**, *90*, 434–444. [CrossRef]
8. Nishikawa, S.; Ooi, K.; Takahashi, M.; Furukawa, T. Influence of shot peening and thermal ageing treatment on resistance to intergranular corrosion in shielded metal arc weld metal for type 600 nickel base alloy. *Weld. Int.* **2017**, *31*, 837–845. [CrossRef]
9. Lu, J.Z.; Luo, K.Y.; Yang, D.K.; Cheng, X.N.; Hu, J.L.; Dai, F.Z.; Qi, H.; Zhang, L.; Zhong, J.S.; Wang, Q.W.; et al. Effects of laser peening on stress corrosion cracking (SCC) of AISI 304 austenitic stainless steel. *Corros. Sci.* **2012**, *60*, 145–152. [CrossRef]
10. Lu, Z.M.; Xu, F.; Tang, C.; Cui, Y.; Xu, H.; Mao, J.F. Stress corrosion cracking susceptibility of 304 stainless steel subjected to laser shock peening without coating. *J. Mater. Eng. Perform.* **2021**, *30*, 7163–7170. [CrossRef]
11. Zhou, J.; Retraint, D.; Sun, Z.; Kanouté, P. Comparative study of the effects of surface mechanical attrition treatment and conventional shot peening on low cycle fatigue of a 316L stainless steel. *Surf. Coat. Technol.* **2022**, *349*, 556–566. [CrossRef]
12. Lopez-Ruiz, P.; Garcia-Blanco, M.B.; Vara, G.; Fernández-Pariente, I.; Guagliano, M.; Bagherifard, S. Obtaining tailored surface characteristics by combining shot peening and electropolishing on 316L stainless steel. *Appl. Surf. Sci.* **2019**, *492*, 1–7. [CrossRef]
13. Karthik, D.; Swaroop, S. Laser shock peening enhanced corrosion properties in a nickel based Inconel 600 superalloy. *J. Alloy Compd.* **2017**, *694*, 1309–1319. [CrossRef]

14. Ming, T.Y.; Xue, H.; Zhang, T.; Han, Y.L.; Peng, Q.J. Improving the corrosion and stress corrosion cracking resistance of 316L stainless steel in high temperature water by water jet cavitation peening. *Surf. Coat. Tech.* **2022**, *438*, 128420. [CrossRef]
15. Ming, T.Y.; Peng, Q.J.; Han, Y.L.; Zhang, T. Effect of water jet cavitation peening on electrochemical corrosion behavior of nickel-based alloy 600 in NaCl solution. *Mater. Chem. Phys.* **2023**, *295*, 127122. [CrossRef]
16. Kuang, W.J.; Wu, X.Q.; Han, E.H.; Rao, J.C. The mechanism of oxide film formation on alloy 690 in oxygenated high temperature water. *Corros. Sci.* **2011**, *53*, 3853–3860. [CrossRef]
17. Feng, H.; Dai, J.; Li, H.B.; Jiang, Z.H.; Qu, J.D.; Zhao, Y.; Zhang, S.C.; Zhang, T. Sn microalloying enhances corrosion resistance of stainless steel by accelerating heterogeneous nucleation of passive film. *Corros. Sci.* **2022**, *201*, 110279. [CrossRef]
18. Huang, R.; Han, Y. The effect of SMAT-induced grain refinement and dislocation on the corrosion behavior of Ti-25Nb-3Mo-3Zr-2Sn alloy. *Mater. Sci. Eng. C* **2013**, *33*, 2353–2359. [CrossRef] [PubMed]
19. Chen, X.D.; Li, Y.S.; Zhu, Y.T.; Bai, Y.K.; Yang, B. Improved corrosion resistance of 316LN stainless steel performed by rotationally accelerated shot peening. *Appl. Surf. Sci.* **2019**, *481*, 1305–1312. [CrossRef]

Disclaimer/Publisher's Note: The statements, opinions and data contained in all publications are solely those of the individual author(s) and contributor(s) and not of MDPI and/or the editor(s). MDPI and/or the editor(s) disclaim responsibility for any injury to people or property resulting from any ideas, methods, instructions or products referred to in the content.